J|A|C|S
ARTICLES
Published on Web 09/15/2006

Sorptive Reconstruction of $CuMCl_4$ (M = Al and Ga) upon Small-Molecule Binding and the Competitive Binding of CO and Ethylene

Michael D. Capracotta, Roger M. Sullivan, and James D. Martin*

Contribution from the Department of Chemistry, North Carolina State University, Raleigh, North Carolina 27695-8204

Received May 12, 2006; E-mail: jdmartin@ncsu.edu

Abstract: Carbonyl adducts to $CuMCl_4$ (M = Al and Ga) have been characterized by single-crystal and/or powder X-ray diffraction, IR and diffuse reflectance UV/vis spectroscopy. Up to two equivalents of carbon monoxide (~200 cm^3/g relative to stp) are sorbed at room temperature, with equilibrium binding pressures of below 0.5 atm of CO. The carbonyl bonding is shown to be nonclassical, implicating the dominance of σ-bonding and absence of π-back-bonding. Analysis of the crystalline structures of the parent and adduct phases provides an atomistic picture of the sorptive reconstruction reaction. Comparison of the reactivity of CO and ethylene with these $CuMCl_4$ materials, as well as other copper(I) halide compounds that exhibit classical and nonclassical modes of bonding, demonstrates the ability to tune the reactivity of the crystalline frameworks with selectivity for carbon monoxide or olefins, respectively.

Introduction

Compounds of copper (I) are well-known to be useful in separations and catalysis applications due to their ability to readily bind small molecules such as olefins, aromatics, and carbonyls.[1−7] Among these, systems that combine Cu(I) with more Lewis acidic metals are the active components in several chemically and economically important processes. For instance Cu(I)/ZnO catalyzes the synthesis of methanol from syngas,[8] and aromatic solutions of CuCl and $AlCl_3$ selectively remove CO from gas mixtures in the COSORB process.[9] Despite the significance of these reaction systems, details of the small-molecule binding remain poorly characterized with respect both to the identity of the active copper species and to the specific role of any additional Lewis acid. We have previously described the solid-state sorptive reconstruction of $CuAlCl_4$ upon reaction with ethylene from an atomistic perspective, in which up to 2 mol equival can be reversibly bound under mild conditions.[2] We demonstrated that in contrast to CuCl, which exhibits a room-temperature ethylene dissociation pressure of 8 atm,[10] addition of $AlCl_3$ facilitates ethylene binding to Cu(I), resulting in dissociation pressures of less than 20 Torr. Unlike ethylene, CO is well-known to bind to CuCl.[11,12] Although sorption is facile for solutions of CuCl in aqueous and organic solvents under 1 atm of CO,[13] sorption into crystalline CuCl requires higher pressures ranging from 3 to 100 atm, depending on particle size.[12,14] The common adduct (CO)CuCl, formed from either solution- or solid-state reactions, exhibits a room-temperature dissociation pressure of 0.5 atm.[14] On the basis of their respective dissociation pressures CO appears to bind more strongly to CuCl than does ethylene, consistent with a classical carbonyl bonding model.[15] However, when in a Lewis acidic environment, CO and olefin binding to Cu(I) has been observed to exhibit nonclassical, i.e., dominated by σ-interactions with little to no π-back-bonding, behavior.[2,5,16−19] Given that CO is a better π-acceptor than ethylene but a slightly weaker σ-donor,

(1) *Separation Technologies for the Industries of the Future*; National Research Council (U.S.A.); 1998, National Academy Press: Washington D.C.
(2) Sullivan, R. M.; Liu, H.; Smith, S.; Hanson, J. C.; Osterhout, D.; Ciraolo, M.; Grey, C. P.; Martin, J. D. *J. Am. Chem. Soc.* **2003**, *125*, 11065−11079.
(3) (a) Turner, R. W.; Amma, E. L. *J. Am. Chem. Soc.* **1966**, *88*, 1877−82. (b) Dattelbaum, A. M.; Martin, J. D. *Inorg. Chem.* **1999**, *38*, 6200−6205. (c) Dattelbaum, A. M.; Martin, J. D. *Polyhedron* **2006**, *25*, 349−359.
(4) Bigorgne, M. *J. Organomet. Chem.* **1978**, *160*, 345−356.
(5) Hadjiivanov, K.; Kantcheva, M. M.; Klissurski, D. G. *J. Chem. Soc., Faraday Trans.* **1996**, *92*, 4595−4600.
(6) Szanyi, J.; Paffett, M. T. *J. Catal.* **1996**, *164*, 232−245.
(7) Bruce, M. I. *J. Organomet. Chem.* **1972**, *44*, 209−226.
(8) (a) Lee, S. *Methanol Synthesis Technology*; CRC Press: Boca Raton, FL, 1990; pp 1−22. (b) Cheng, W. H.; Kung, H. H. Methanol Production and Use; Cheng, W. H., Kung, H. H., Eds.; Marcel Dekker: New York, 1994; pp 1−22.
(9) (a) Haase, D. J.; Walker, D. G. *Chem. Eng. Prog.* **1974**, *70*, 74−77. (b) Long, R. B.; Caruso, F. A.; Walker, D. G. Monomere Bimetellsalze sowei Verfahren zu ihrer Herstellung and Verbindung. German Patent DE 1,-944,405, 1968. (c) Turnbo, R. G. Process for the Preparation of Bimetallic Salt Complexes. U.S. Patent 3,857,869, 1974. (d) Sudduth, J. R.; Keyworth, D. A. Process for the Purification of Gas Streams. U.S. Patent 3,960,910, 1975. (e) Walker, D. G. *Chem. Technol.* **1975**, *5*, 308−311.
(10) Gilliland, E. R.; Seebold, J. E.; FitzHugh, J. R.; Morgan, P. S. *J. Am. Chem. Soc.* **1939**, *61*, 1960−1962.
(11) (a) Leblanc, F. *C. R. Acad. Sci. Paris* **1850**, *30*, 483. (b) Berethelot, M. *Ann. Chim. Phys.* **1856**, *346*, 364.
(12) Wagner, O. H. *Anorg. Allg. Chem.* **1931**, *196*, 364−373.
(13) (a) Backen, W.; Vestin, R. *Acta Chem. Scand.* **1979**, *A33*, 85−91. (b) Hakansson, M.; Jagner, S. *Inorg. Chem.* **1990**, *29*, 5241−5244. (c) Pasquali, M.; Florinani, C.; Gaetani-Manfredotti, A. A. *Inorg. Chem.* **1981**, *20*, 3382−3388.
(14) Peng, X. D.; Golden, T. C.; Pearlstein, R. M.; Pierantozzi, R. *Langmuir* **1995**, *11*, 534−537.
(15) Huang, H. Y.; Padin, J.; Yang, R. T. *Ind. Eng. Chem. Res.* **1999**, *38*, 8, 2720−2725.
(16) Strauss, S. H. *J. Chem. Soc., Dalton Trans.* **2000**, 1−6.
(17) Rack, J. J.; Webb, J. D.; Strauss, S. H. *Inorg. Chem.* **1996**, *35*, 277−278.
(18) Willner, H., and Aubke, F. *Angew. Chem., Int. Ed. Engl.* **1997**, *36*, 2402−2425.
(19) Brand, H. V.; Redondo, A.; Hay, P. J. *J. Phys. Chem. B* **1997**, *101*, 7691−7701.

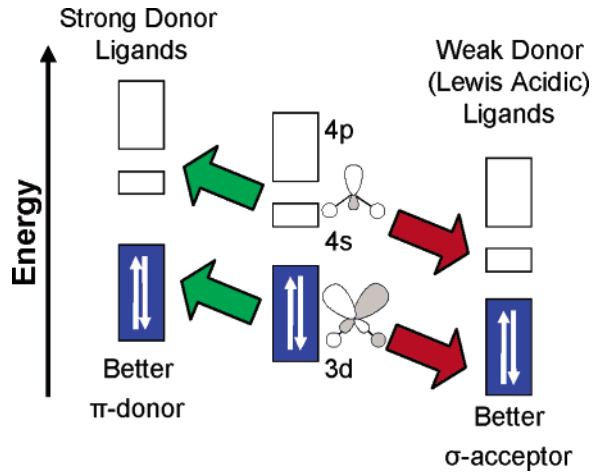

Figure 1. Schematic representation of the ligand influence on the copper-(I) frontier orbitals. Given that both occupied Cu 3d and unoccupied Cu 4s and 4p orbitals are metal−ligand antibonding, strong donor ligands destabilize these orbitals making the system a better π-donor, whereas weak donor ligands stabilize these orbitals making the system a better σ-acceptor.

a study of the comparative binding of CO and ethylene to CuCl, and $CuMCl_4$ (M = Al and Ga) was initiated to probe bonding and mechanistic details of small-molecule binding to Cu(I) in a Lewis acidic coordination environment. Specifically in this report we describe the pressure-resolved synchrotron diffraction and spectroscopic characterization of one and two equivalent carbonyl adducts to $CuMCl_4$ (M = Al and Ga), as well as the single-crystal structure of the 1 equiv adduct, $(CO)CuAlCl_4$. These data, along with our previous report on ethylene binding demonstrate the ability to fine-tune the specific reactivity of Cu(I)-based materials.

Background

The electronic structure of Cu(I) makes it well suited to be the active site for reversible binding of small molecules such as olefins and carbon monoxide. Since copper has an electronegativty similar to that of silicon, Cu−Cl bonds must have significant covalent character. With a d^{10}-electronic configuration, the relatively high-lying HOMO consists of M−L σ* character. However, the empty s- and p-orbitals of copper (I), also of M−L σ* character, are quite low in energy, resulting in a very small HOMO−LUMO gap. These low-lying empty metal-based orbitals readily mix with the HOMO in a second-order Jahn−Teller fashion, which results in an extensive geometric flexibility of the copper (I) coordination sphere.[20] These frontier orbitals also dictate the reactivity of many copper complexes. In both four- and three-coordinate geometries the M−L σ* HOMOs possess appropriate symmetry to back-bond in a π-fashion, whereas the symmetry of the metal s/p-based LUMO is appropriate for σ-acceptor interactions. Strong ancillary donor ligands destabilize all of these orbitals, which enhance the metal's ability to π-back-bond and make it a less effective σ-acceptor, as shown in the left portion of Figure 1. Nature has exploited this mode of binding enhancement with strong amine-type ligands bound to copper in ethylene-binding metalloenzymes.[21] However, in the presence of weak donor ligands, such as the conjugate base of strong Lewis acids (i.e., $AlCl_4^-$, AsF_6^-), these frontier orbitals are stabilized, providing a better σ-acceptor configuration with little to no back-bonding ability,[2,5,16−19] represented on the right-hand side of Figure 1 and described as nonclassical.

Table 1. Summary of Cu(I)−Monocarbonyl Stretching Frequencies

	material/complex	ν_{CO} (cm^{-1})	ref
a.	(dipyam)Cu(CO)Cl[a]	2069	25
b.	(en)Cu(CO)Cl[b]	2080	26
c.	DCEACu(CO)Cl[c]	2096	27
d.	(CO)CuCl (MeOH solution)	2070	13c
e.	(CO)CuCl	2127	13b
f.	(CO)CuCl (100 K)	2134−2136	23
g.	Cu(CO)Cl (Ar matrix)	2157	24
h.	$(CO)CuAlCl_4$	2156	this work
i.	$(CO)CuGaCl_4$	2156	this work
j.	Cu(I)/ZnO	2103	28
k.	Cu_2O	2127	29
l.	Cu_2O/SiO_2	2132	29
m.	Cu(I)−ZSM-5	2157	30
n.	Cu(I)−mordenite	2159	31
o.	$(CO)Cu(O_2CCF_3)$	2155	32
p.	$[(CO)Cu][1\text{-Et-}CB_{11}F_{11}]$	2175	33
q.	$[(CO)Cu][AsF_6]$	2178	17
r.	$[(CO)Cu]^+$ Ne/CO matrix	2234	34

[a] dipyam = 2,2′-dipyridylamine. [b] en = ethylenediamine. [c] DCEA = bis(2-cyanoethyl)amine.

The carbonyl stretching frequency of a carbon monoxide ligand bound to a metal center is a sensitive measure of the relative classical/nonclassical nature of ligand binding.[16−19] With its HOMO being a σ-lone pair with weak C−O antibonding character[22] and its LUMO being the C−O π* orbital, classical M−CO binding (i.e. with significant π-back-bonding) results in a decrease of the CO stretching frequency from that of free CO, 2143 cm^{-1}. By contrast, nonclassical bonding (i.e. predominately σ-bonding) results in a small increase in the CO stretching frequency. (It is important to recognize that π-back-bonding into the CO π* orbital has a much greater effect on the ν_{CO} than does σ-donation from the weakly antibonding CO lone pair.[22b]) As observed from the tabulation of CO stretching frequencies presented in Table 1, chloride ligands for Cu(I)−CO complexes create an environment that appears to sit very nearly at the classical/nonclassical boundary, with ν_{CO} = 2127 for (CO)CuCl. Interestingly, at 100 K, a thin film of (CO)CuCl exhibits a slight strengthening of the ν_{CO} = 2135 (Table 1, f),[23] and matrix isolating the (CO)CuCl complex results in nonclassical bonding with ν_{CO} = 2157 cm^{-1}.[24] These data indicate very minimal dπ−COπ* interaction for the chloride complex. The addition of donor ligands, such as amines, to a copper chloride carbonyl complex (Table 1, a−c) pushes the Cu−CO bonding toward the classical mode. Placing the copper (I) center in a more Lewis acidic environment such as in a zeolite (Table 1 m,n) or complexed with a noncoordinating anion (Table 1, o−q) clearly shifts copper−carbonyl bonding to the nonclassical motif. The matrix-isolated cation $[(CO)Cu]^+$ (Table 1, r) provides the limiting value for nonclassical binding.[34]

(20) Burdett, J. K.; Eisenstein, O. *Inorg. Chem.* **1992**, *31*, 1758−1762.
(21) Rodríguez, F. I.; Esch, J. J.; Hall, A. E.; Binder, B. M.; Schaller, G. E.; Bleeker, A. B. *Science* **1999**, *283*, 996−998.
(22) (a) Das, B.; Sebastian, K. L.; Samuelson, A. G. *J. Mol. Struct. (THEOCHEM)* **2005**, *730*, 69−83. (b) Lupinetti, A. J.; Fau, S.; Frenking, G.; Strauss, S. H. *J. Phys. Chem. A* **1997**, *101*, 9551−9559. (c) Goldman, A. Krogh-Jespersen, K. *J. Am. Chem. Soc.* **1996**, *118*, 12159−12166.
(23) Scarano, D.; Galletto, P.; Lamberti, C.; De Franceschi, R.; Zecchina, A. *Surf. Sci.* **1997**, *387*, 236−242.
(24) (a) Plitt, H. S.; Bär M. R.; Ahlrichs, R.; Schnöckel H. *Inorg. Chem.* **1992**, *31*, 463−465. (b) Shao, L.; Zhang, L.; Zhou, M.; Qin, Q. *Organomet.* **2001**, *20*, 1137−1143.
(25) Ugozzoli, F.; Lanfredi, A. M. M.; Marisch, N.; Camus, A. *Inorg. Chim. Acta* **1997**, *256*, 1−7.

The ligand environment thus clearly tunes the binding affinity of copper (I). Many Lewis basic donor ligands exist (i.e., amines and phosphines) that enhance the classical mode of bonding. By contrast, tuning a complex toward nonclassical bonding is more complicated, since Lewis acidic ligands (with the exception of π-acids) essentially do not exist. Here we utilize a strategy whereby a common-ion Lewis acid tunes the ligand field around the metal center (eq 1) so as to enhance nonclassical bonding.

$$MCl_n + CuCl \rightarrow CuMCl_{n+1} \qquad (1)$$

The reactivity of copper chloride toward CO and ethylene in the presence of the common-ion Lewis acids $AlCl_3$ and $GaCl_3$ clearly demonstrate this enhanced nonclassical bonding. Mono- and dicarbonyl adduct phases (CO)$CuMCl_4$, **1-CO$_M$** and $(CO)_2$-$CuMCl_4$, **2-CO$_M$**, (M = Al and Ga) have been characterized by gravimetric and volumetric sorption, FTIR and UV/vis spectroscopy, and pressure-resolved synchrotron diffraction studies. These data, correlated with previously reported data,[2] demonstrate the ability to fine-tune the copper (I) reactivity so as to favor carbon monoxide vs olefin binding. The structural data provide further insight into our ongoing mechanistic study of the reconstruction of the $CuMCl_4$ lattice upon small-molecule sorption.

Results

Adsorption Isotherm Measurements. Volumetric and gravimetric experiments were performed to probe the sorptive capabilities of $CuAlCl_4$ and $CuGaCl_4$ with CO. Exposure of a bulk sample of $CuAlCl_4$ to 1500 Torr of CO at room temperature results in loss of the material's characteristic blue-green luminescence[35] and uptake of approximately 1 equiv of CO, as measured gravimetrically. Up to about 1 atm of CO pressure, the material remains solid. However, upon increasing the CO pressure, a eutectic melt-type behavior is observed with the fraction of amber-colored liquid increasing with increasing CO pressure. Exposing the solid or liquid products to dynamic vacuum results in a reversion to a solid phase. The return of luminescence upon desorption is indicative of reformation of the parent $CuAlCl_4$. However, even after evacuation for several hours at room temperature, gravimetric analysis shows that approximately 0.2 equiv of CO remain sorbed. Heating the solid to its melting temperature, approximately 45 °C, under vacuum removes all of the remaining CO with quantitative reformation of crystalline α-$CuAlCl_4$ (mp = 235 °C). Carbon monoxide can also be removed from the solid adduct by grinding under an N_2 atmosphere in a glovebox. Similar results are observed by exposing $CuGaCl_4$ to CO; however, no liquid phase is observed upon CO sorption, and the adduct phases decompose prior to melting.

(26) Rucci, G.; Zanzottera, C.; Lachi, M. P.; Camia, M. *Chem. Commun.* **1971**, *12*, 652.
(27) Balkus, K. J., Jr.; Kortz, A.; Drago, R. S. *Inorg. Chem.* **1988**, *27*, 2955−2958.
(28) Bocuzzi, F.; Ghiotti, G. *J. Phys., Colloq.* **1983**, *C10*, 455−458.
(29) Scarano, D.; Bordiga, S.; Lamberti, C.; Spoto, G.; Ricchiardi, G.; Zecchina, A.; Otero Arean, C. *Surf. Sci.* **1998**, *41*, 272−285.
(30) Hadjiivanov, K. I.; Kantcheva, M. M.; Klissurski, D. G. *J. Chem. Soc., Faraday Trans.* **1996**, *92*, 4595−4600.
(31) Lamberti, C.; Bordiga, S.; Zecchina, A.; Salvaleggio M.; Geobaldo, F.; Otero Areán, C. *J. Chem. Soc., Faraday Trans.* **1998**, *94*, 1519−1525.
(32) Scott, A. F.; Wilkening, L. L.; Rubin B. *Inorg. Chem.* **1969**, *8*, 2533−2534.
(33) Ivanova, S. M.; Ivanov, S. V.; Miller, S. M.; Anderson, O. P.; Solntsev, K. A.; Strauss, S. H. *Inorg. Chem.* **1999**, *38*, 3756−3757.
(34) Zhou, M.; Andrews. L. *J. Chem. Phys.* **1999**, *111*, 4548−4557.
(35) Sullivan, R. M.; Martin, J. D. *J. Am. Chem. Soc.* **1999**, *121*, 10092−10097.

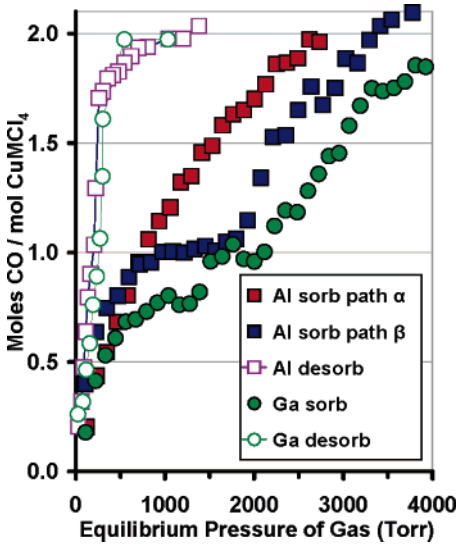

Figure 2. Representative sorption−desorption isotherms for the systems $CuAlCl_4$ + CO and $CuGaCl_4$ + CO.

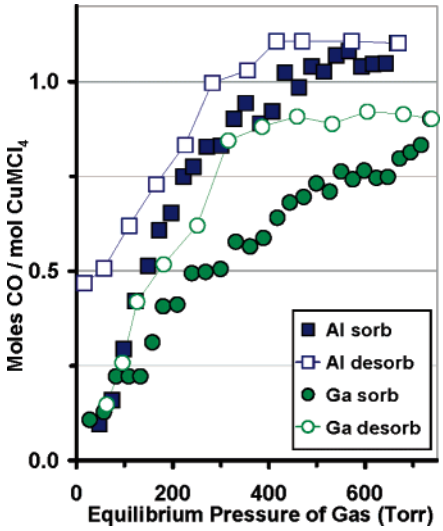

Figure 3. Sorption−desorption isotherms for the 1 equiv phases from the $CuAlCl_4$ + CO and $CuGaCl_4$ + CO systems.

Representative examples of volumetric sorption/desorption isotherms are given in Figures 2 and 3, plotted as the number of moles of CO sorbed per mole of $CuMCl_4$ vs the equilibrated pressure of CO. Sorption isotherms were measured using variously sized steps in CO pressure of 50−600 Torr in an attempt to access multiple reaction pathways as observed previously for ethylene sorption.[2] However, neither the initial exposure pressure nor the size of the sorption steps appeared to have any significant effect on the sorption reaction. Nevertheless, two characteristic patterns of reactivity, described as path α and β, respectively (according to the crystalline polymorph formed by each as described below), were observed for the sorption isotherms into $CuAlCl_4$, shown in Figure 2. The β path exhibits a plateau at approximately 1 equiv and around 1 atm of CO pressure, consistent with the formation of (CO)$CuAlCl_4$, **1-CO$_{Al}$**, followed by gradual sorption to 2 equiv of CO, to form $(CO)_2CuAlCl_4$, **2-CO$_{Al}$**, at an equilibrium pressure of 4000 Torr. By contrast, the α path appears to form the higher adduct at lower pressures and does not exhibit a plateau at 1 equiv. Five out of 10 isotherm measurements were observed to follow each

type of reaction path. We have not yet been able to determine what factors determine which reaction path will be followed. Carbon monoxide sorption into $CuGaCl_4$ has only been observed to follow the stepwise β-type path. For sorption into $CuGaCl_4$, the initial plateau occurs with only about 0.75 equiv of CO sorbed, assigned to the incomplete formation of **1-CO$_{Ga}$**. With increasing pressure, however, 2 equiv of CO are sorbed when the equilibrium pressure of 4000 Torr is achieved, corresponding to the formation of **2-CO$_{Ga}$**. Similar experiments were performed with CuCl (data not shown), but no sorption of CO was observed up to equilibrated pressures of 4000 Torr, consistent with literature reports.[12,14]

Significant hysteresis is observed between the sorption and desorption of CO into both $CuMCl_4$ materials. No CO desorption is observed until pressures below 1 atm are achieved. Desorption from **2-CO$_{Al}$** commences at an equilibrium pressure of about 700 Torr. Desorption from **2-CO$_{Ga}$** occurs at a slightly lower pressure, 500 Torr, although a precise comparison is outside the limits of our experiential apparatus. A second series of sorption/desorption experiments in which only the 1 equiv adducts were allowed to form (Figure 3) demonstrates less dramatic hysteresis than was observed for the 2 equiv adducts. The desorption pressure for **1-CO$_{Al}$** (determined by the intersection of the higher pressure plateau, and the approximately linear slope for desorption between about $0.8 > \alpha > 0.5$) is about 360 Torr and that for **1-CO$_{Ga}$** is about 330 Torr. Again, while the experimental apparatus does not allow precise measurement of the desorption pressure, repeatedly, **1-CO$_{Ga}$** samples retain CO to slightly lower pressures than does **1-CO$_{Al}$**. In these room-temperature experiments, complete desorption is never achieved, leaving between 0.15 and 0.45 mol of sorbed gas, depending on the individual experiment.

Synchrotron Powder X-ray Diffraction. In situ synchrotron powder X-ray diffraction experiments were conducted to identify the phases present in the reactions of $CuAlCl_4$, $CuGaCl_4$, and CuCl with CO. As there is a significant pressure gradient along the capillary tubes used in these experiments, it is not possible to draw a precise comparison between the sorption isotherms and the diffraction measurements. The pressure gradient can be inferred by the observation that more CO-rich products are present at the end of the capillary closest to the gas exposure. This problem is somewhat alleviated by mixing the reactive metal halide with ground fused silica as an inert matrix that helps allow the CO to diffuse through the capillary. Also melting the $CuAlCl_4$ in the presence of the silica matrix, followed by subsequent cooling to room temperature, gives a thin film of material over the ground silica that increases its surface area and promotes reaction. In experiments without the fused silica, product phases were normally only observed within the first 1−3 mm of the sample, while little or no reaction occurred deeper into the capillary. A summary of the characteristic low-angle reflections that identify each of the phases is given in Table 2.

Starting with a $CuAlCl_4/SiO_2$ mixture cooled to 15 °C and under vacuum, the pressure of CO was gradually increased over a period of approximately 90 min (i.e. 10 min equilibration at each pressure). Figure 4 shows the time/pressure-resolved X-ray diffraction data for this reaction. At a pressure of 860 Torr (Figure 4b), diffraction peaks indicative of α-**1-CO$_{Al}$** are observed along with peaks corresponding to **2-CO$_{Al}$**. The intensity of the peaks corresponding to α-**1-CO$_{Al}$** grow with increasing pressure until pressures of greater than 2000 Torr are achieved (Figure 4e), at which point they begin to decrease in intensity. As the pressure is increased, peaks corresponding to **CuAlCl$_4$** and α-**1-CO$_{Al}$** continue to diminish, while peaks for **2-CO$_{Al}$** grow only slightly. Further progress of the reaction to the maximum experimental pressure of 4500 Torr shows an increase in the amorphous background consistent with the formation of a eutectic melt. In sorption experiments with only **CuAlCl$_4$** loaded in the capillary (i.e. no ground fused silica), only a partial reaction to form **1-(CO)$_{Al}$** is observed even at the maximum experimental pressure of gas. Such reactions normally exhibited evidence of the β-**1-CO$_{Al}$** phase. (See Supporting Information, Figure S1). Sorption experiments into **CuGaCl$_4$**

Table 2. Characteristic Low-Angle Reflections for Identifying Phases in Powder X-ray Diffractograms

phase	*hkl*	Q (Å^{-1})[a]
α-$CuAlCl_4$	100	1.15
	002	1.24
	101	1.31
α-(CO)$CuAlCl_4$	100	0.59
α−1-CO$_{Al}$	110	1.01
	011	1.06
β-(CO)$CuAlCl_4$	001	0.77
β−1-CO$_{Al}$	100	0.97
	101	1.02
$(CO)_2CuAlCl_4$	010	0.53
2-CO$_{Al}$	100	0.68
	−110	0.94

[a] Data are reported as a function of the wavelength independent Q instead of 2θ in order to readily compare data collected using various X-ray sources. $Q = (4\pi \sin(\theta))/\lambda$.

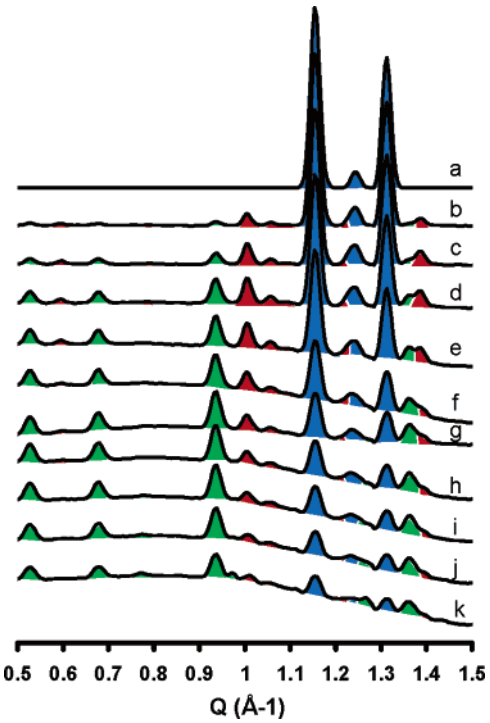

Figure 4. Variable pressure X-ray diffraction showing the conversion of α-$CuAlCl_4$ to $(CO)_2CuAlCl_4$ at (a) 0, (b) 860, (c) 1000, (d) 1500, (e) 2000, (f) 2500, (g) 3000, (h) 3500, (i) 4000, (j and k) 4500 Torr of CO. The sample was equilibrated at each pressure for 10 min. The powder patterns are color-coded blue for α-$CuAlCl_4$, red for α-(CO)$CuAlCl_4$ and for $(CO)_2$-$CuAlCl_4$.

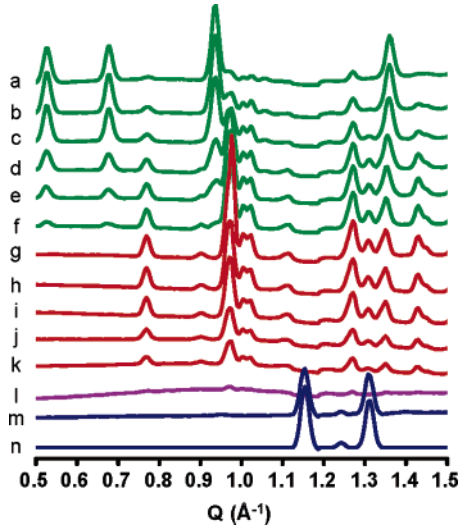

Figure 5. Time/temperature-resolved X-ray diffraction for the desorption of CO from $(CO)_2CuAlCl_4$ [(diffractogram) temperature in °C]: (a) $(CO)_2CuAlCl_4$ (green line): 25. Desorption to form $(CO)CuAlCl_4$: (b) 26, (c) 27, (d) 29, (e) 30, (f) 31. Pure $(CO)CuAlCl_4$ (red lines): (g) 32, (h) 36, (i) 43, (j) 45, (k) 50, (l). Melted $(CO)CuAlCl_4$ (purple line): 53. Desorption to give $CuAlCl_4$ (blue lines): (m) 57, (n) 61. The sample was heated under vacuum from 25 to 45 °C at a rate of 0.25 °/min then 45−100 °C at a rate of 1°/min. A diffractogram was taken every 1.2 min, selections of which are shown.

exhibit similar behavior, except that reactions do not proceed as far toward completion under the accessible CO pressure, and no sample melting is observed (Supporting Information Figure S2). Here, β-**1-CO$_{Ga}$** is the only product initially observed, and partial formation of **2-CO$_{Ga}$** is only observed at higher CO pressure. Unfortunately, we have not been able to achieve complete formation of β-**1-CO** prior to formation of **2-CO** as would seem to be implied by the β path sorption isotherm of Figure 2.

As shown in Figure 5, a stepwise desorption of CO from **2-CO$_{Al}$** is observed as the capillary is heated under vacuum. To date, only the β-**1-CO$_{Al}$** has been observed upon desorption, whereas both the α- and β-phases have been observed upon sorption. At about 45 °C β-**1-CO$_{Al}$** begins to melt. At 53 °C the adduct phase is completely melted and begins to release CO resulting in the reformation of crystalline $CuAlCl_4$ starting material. Heating to 100 °C under vacuum resulted in complete desorption of the adduct phase, leaving only crystalline α-$CuAlCl_4$. Desorption of CO from β-**1-CO$_{Ga}$** also requires heating, although the CO is lost prior to sample melting.

While sorption of CO into $CuAlCl_4$ results in a unit cell volume expansion of 130% and 190% to form **1-CO** and **2-CO**, respectively, these reactions interestingly do not cause fragmentation of the reactant crystallites into nanoparticulate products, even upon multiple sorption/desorption cycles. Two-dimensional (2-D) diffraction images, Figure 6, provide interesting insight as to particle size effects of the sorptive reconstruction reactions. Note: a sample consisting of a fine random powder exhibits smooth diffraction rings, whereas a sample with coarser particle size exhibits spotty rings. Frames a and b of Figure 6 demonstrate that coarse-grained products are formed upon sorption into $CuAlCl_4$ and $CuGaCl_4$, respectively. A significant amorphous ring for the **1-CO$_{Al}$/2-CO$_{Al}$** eutectic melt is also clearly observed in Figure 6a. The "grainyness" of these product diffraction patterns is relatively independent of the

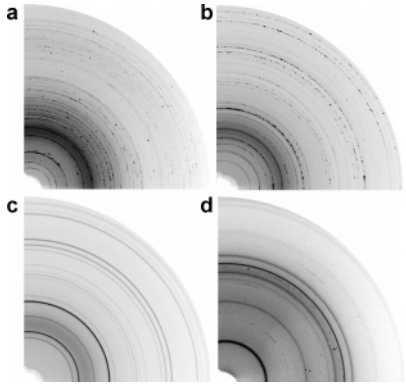

Figure 6. Quarter-image plates from PRXRD of reaction of **$CuMCl_4$** + CO. (a) Grainy diffraction pattern of **2-CO$_{Al}$** with amorphous diffraction ring from the eutectic melt. (b) Grainy diffraction pattern with a mixture of **2-CO$_{Ga}$**, β-**1-CO$_{Ga}$**, and α-**$CuGaCl_4$**. (c) Microcrystalline α-**$CuGaCl_4$** from desorption of CO from (b). (d) Nanocrystalline diffraction pattern of **(CO)CuCl**.

particle size of the starting reactants (∼10 μm to 0.1 mm). By contrast, upon desorption and reconstruction of the parent $CuMCl_4$ phase, a very fine-grained powder is formed as shown by the diffraction image of Figure 6c, although this pattern gives no evidence of Scherrer line-broadening.

When capillaries of either $CuAlCl_4$ or $CuGaCl_4$ are not sealed well on the gas line, a small amount of air/moisture is able to reach the sample. When this occurs, the diffraction pattern for the previously characterized (CO)CuCl[13b] grows in upon exposure to CO. This capillary reaction proceeds to completion in approximately 30 min at a pressure of 4000 Torr. When (CO)-CuCl is formed, no additional diffraction peaks are observed, precluding identification of the Al- and Ga-containing products. Presumably, some amorphous phase on the way toward $MCl_3 \cdot 6H_2O$ is formed. Unlike the formation of **1-CO$_{Al}$** and **1-CO$_{Ga}$**, the 2-D image plates of (CO)CuCl exhibit fine powder rings (Figure 6d), demonstrating that this reaction is extremely destructive to the crystalline lattice. Significant line broadening, about 0.015 Å^{-1}, is observed for the powder pattern(s) of (CO)-CuCl (and CuCl after desorption) consistent with nanocrystalline particle size (∼40 nm). Equivalent pressure-resolved diffraction experiments with CuCl ground in an agate mortar and pestle (∼10 μm particle size) show no evidence of carbon monoxide sorption. The CuCl−CO adduct loses CO when placed under vacuum, and the combination of vacuum and mild heating (approximately 50 °C) yields nanoparticulate CuCl. Reexposure of the nanoparticulate CuCl to CO results in the reformation of (CO)CuCl, consistent with the previously reported particle size dependence of this reaction.[14]

X-ray Crystal Structures. Single crystals of β-**1-CO$_{Al}$** were grown in situ by melt recrystallization in a capillary under a pressure of CO, and its crystal structure was determined by X-ray diffraction. The structure of the isomorphous β-**1-CO$_{Ga}$** was refined by Rietveld analysis of synchrotron X-ray powder diffraction data. It has not yet been possible to determine the structures of the α-**1-CO$_{Al}$** and **2-CO$_{Al}$** phases; nevertheless, lattice constants for these phases have been determined by powder diffraction methods using analogous ethylene adduct phases as starting model structures. A summary of the crystallographic data is given in Table 3. Full details of the structure solution are available in the Supporting Information.

Table 3. Summary of Crystal Data for $(CO)_xCuMCl_4$ Adducts

formula	β-$(CO)CuAlCl_4$	α-$(CO)CuAlCl_4$	β-$(CO)CuGaCl_4$	$(CO)_2CuAlCl_4$
	***β*-1-CO$_{Al}$**	**α-1-CO$_{Al}$**	***β*-1-CO$_{Ga}$**	**2-CO$_{Al}$**
	single crystal	powder	powder	powder
formula weight	260.33	260.33	303.07	288.34
temp (°C)	25	15	15	15
space group	$P\bar{1}$ (2)		$P\bar{1}$ (2)	
a (Å)	6.8752(3)	10.67(1)	6.877(1)	9.62(4)
b (Å)	7.0092(3)	7.664(6)	7.015(1)	12.23(6)
c (Å)	8.7362(3)	9.389(5)	8.759(2)	5.152(4)
α (deg)	81.798(2)	90	81.00(2)	98.8(2)
β (deg)	69.646(2)	93.2(1)	69.45(1)	101.6(5)
γ (deg)	85.723(2)	90	85.73(2)	99.1(7)
V (Å^3)	390.53(2)	767(1)	390.75(9)	576(4)
Z	2		2	
R	0.0341		0.0551	
R_w	0.0941		0.0893	

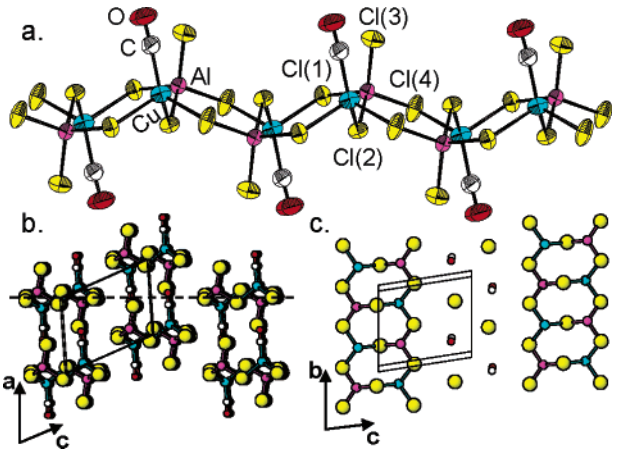

Figure 7. (a) ORTEP (50% probability ellipsoid) of a chain of β-1-CO showing the atom labeling scheme. (b) A crystal packing view of the crystal structure looking down the chains (along **b**). (c) A view of the pseudo-close packing of the chlorides and carbonyl ligands in the (201) planes. The (201) plane is also represented with the dashed line in (b).

The structure of ***β*-1-CO$_{Al}$** exhibits a ladder-type chain running along **b**, with Cu−Cl−Al rungs that are connected through chloride bridges and related by inversion symmetry, as shown in the ORTEP drawing of Figure 7. This results in a strict alternation of corner-shared copper and aluminum tetrahedra. The chains are puckered with the metal cations filling tetrahedral interstices on alternating sides of an anion layer composed of both rung- and rail-bridging chlorides. Carbonyl ligands are terminally bound to each copper site with a near linear coordination geometry (Cu−C−O = 175.89(3)°) at a distance of Cu−C = 1.857(3) Å. The carbonyl and the three chloride bridges (Cu−Cl(1) = 2.4597(7) Å, Cu−Cl(2) = 2.3737(7) Å, and Cu−Cl(4) = 2.3910(7) Å) form a somewhat distorted tetrahedron about the copper, with contracted angles for the chloride face (Cl(1)−Cu−Cl(4) = 95.86(3)°, Cl(1)−Cu−Cl(2) = 103.67(3)°, and Cl(2)−Cu−Cl(4) = 101.59(3)°) and expanded angles about the carbonyl ligand (C−Cu−Cl(2) = 124.52(9)°, C−Cu−Cl(1) = 107.33(9)° and C−Cu−Cl(4) = 119.28(10)°). The geometry about the tetracholoroaluminate is a more regular tetrahedron, although the relatively short terminal bond, Al−Cl(3) = 2.090(1) Å, with respect to the slightly longer bonds to bridging chlorides (Al−Cl(1) = 2.1443(9) Å, Al−Cl(2) = 2.1673(9) Å, and Al−Cl(4) = 2.1508(9) Å) causes a distortion away from the terminal chloride. The average Cl−Al−Cl bond angle to the terminal ligand is 111.7°, whereas the average bond angle between the bridging chlorides is 107.2°. Interestingly, the nearly eclipsed CO ligand and terminal chloride exhibit a remarkably short contact, Cl- -C = 3.36 Å, across the ladder rails. This is the shortest interligand contact; the next shortest being Cl(1)- -Cl(4) = 3.45 Å and Cl-(1)- -C = 3.50 Å. These suggest that there may be some across-chain chloride- -π-system interaction, similar to the chloride- -π interaction observed in related structures with ethylene and benzene.[2,36,37]

These $(CO)CuAlCl_4$ chains pack extremely efficiently, with the carbonyl and terminal chlorides from chains related by ±**a** interpenetrating a common layer of ligands, seen in Figure 7, b and c. In fact the CO and Cl^- are so nearly the same size that they form pseudo-close-packed layers with the CO ligands filling one-fifth of the close-packing sites. Each close-packed layer (Figure 7c) consists of all the bridging chloride ligands from chains in a crystallographic (201) plane, and the interpenetrating terminal chloride and carbonyl ligands from chains related by ±**c** and ±(−**a**+**c**). The copper and aluminum cations pairwise fill 2/10 of the tetrahedral interstices on alternating sides of these close-packed planes. These layers are then stacked in a *hcp* fashion. The interdigitation of the CO and terminal chlorides is reminiscent of the packing of the 2-D sheets of (CO)CuCl.[13b]

The structure of the α-1-CO_{Al} remains elusive, but based on the lattice constants and relative diffraction intensities, we propose that it exhibits a structure similar to that of the α-1-et ethylene adduct, previously reported.[2] The ethylene structure also was not well refined but appears to have orthogonal, as opposed to parallel, ladder chains that run through the crystalline structure. Similarly, the structure of the **2-CO** adduct has not yet been determined, but powder patterns and lattice constants suggest a likely similarity to the structure of the **2-et** ethylene adduct, however, with the CO ligands bound end-on as opposed to the edge binding of the ethylene ligands.[2]

FTIR and UV/Vis Spectroscopy. The reactions of $CuMCl_4$ (M = Al and Ga) with CO were monitored by FTIR spectroscopy to determine the carbonyl stretching frequency of the adduct phases. Samples were prepared by reaction of $CuMCl_4$ with CO in either fused silica reaction tubes (Figure 8) or in a flow cell with KBr windows (Supporting Information Figure S3), with both methods yielding similar spectra in the carbonyl stretching region. The fused silica tubes are most readily interfaced with our gas line, and fortunately have a window in the IR spectrum in the vicinity of the observed CO stretching

(36) Dattelbaum, A. M.; Martin, J. D. *Polyhedron* **2006**, *25*, 349−359.
(37) Dattelbaum, A. M.; Martin, J. D. *Inorg. Chem.* **1999**, *38*, 6200−6205.

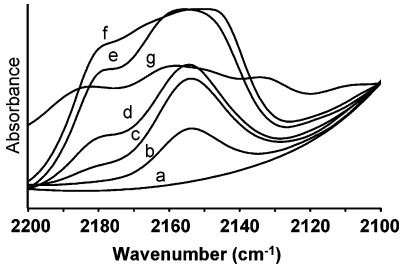

Figure 8. FTIR of CO + $CuAlCl_4$ reaction at (a) 0 Torr, (b) 200 Torr, (c) 375 Torr, (d) 750 Torr, (e) 850 Torr, (f) 950 Torr. Spectrum g is of the eutectic liquid which forms in this system.

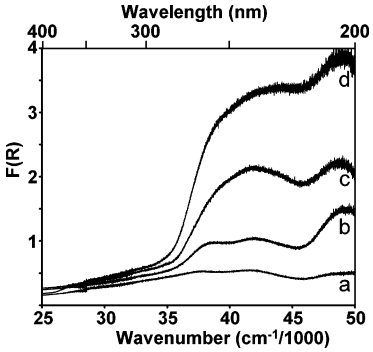

Figure 9. Diffuse reflectance UV−vis of CO + CuAlCl4 reaction at (a) vacuum, (b) 110 Torr, (c) 820 Torr, and (d) 930 Torr.

frequencies; though the window becomes blocked below abut 2100 cm^{-1}. Figure 8 shows spectra from a representative variable-pressure experiment performed in a fused silica tube. At low pressures of CO (200−400 Torr), a single peak is observed in the carbonyl stretching region at 2156 cm^{-1}. As the sample is exposed to increased CO pressure at 750 Torr, this peak increases in intensity, and new features are observed at 2182 and 2107 cm^{-1} (more clearly resolved in Figure S3), likely corresponding to **2-CO_{Al}**. At this and higher pressures (up to 1500 Torr), some of the sample begins to form a translucent, brown liquid phase. An IR spectrum of the liquid separated from the solid material under 950 Torr of CO (Figure 8g) shows the above peaks and an additional band at 2130 cm^{-1}, possibly suggesting a higher carbonyl adduct. Pure $(CO)_2CuAlCl_4$ could not be obtained with this apparatus. Samples of (CO)-$CuGaCl_4$ also show a peak at 2156 cm^{-1} when exposed to CO pressures around 1 atm, with no additional peaks in the carbonyl stretching region observed on increasing pressure to 1500 Torr.

Following the same CO sorptive reconstruction reaction by diffuse reflectance UV/vis spectroscopy probes the electronic structure of the adduct phases (Figure 9). Upon initial sorption under about 110 Torr of CO the relatively weak and broad Cu → CO metal-to-ligand charge-transfer band becomes visible at about $\lambda_{max} = 38.4 \times 10^3$ cm^{-1}, very near to the Cu 3d → Cu 4s transition of the parent $CuAlCl_4$ phase.[35] By way of reference, a very weak Cu → CO charge-transfer band is observed at around $\lambda_{max} = 37.8 \times 10^3$ cm^{-1} for the sorption of CO into CuCl to form (CO)CuCl. Increasing the CO pressure in this UV/vis reaction cell results in the observation of increased absorption, particularly of the broad higher-energy features at 42.1×10^3 and 48.8×10^3 cm^{-1} which we assign to the **2-CO_{Al}** adduct.

Scheme 1

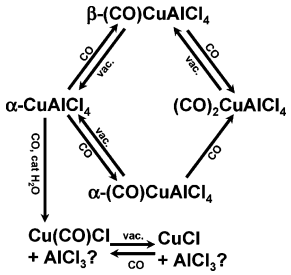

Discussion

The sorption isotherms, X-ray structural studies and spectroscopic measurements give indication of a complex pattern of reactivity between $CuMCl_4$, M = Al and Ga, and CO, summarized in Scheme 1. Both $CuAlCl_4$ and $CuGaCl_4$ reversibly sorb CO gas forming 1 mol equiv adduct phases at less than 0.5 atm of CO and a 2 equiv phase at higher pressures. Like other systems which exhibit a significant swelling of the crystalline structure on sorption, the sorption isotherms for these materials exhibit a significant hysteresis between sorption and desorption.[38] A comparative analysis of the crystal structures of the parent α-$CuMCl_4$ and those of the products **1-CO** and **2-CO** provide an atomistic picture of the sorptive reconstruction process, suggesting that sorption occurs directly at the phase boundary in contrast to sorption into clays where initial sorption opens a gallery into which more gas can be sorbed.[38] Nevertheless the addition of the strong Lewis acids to the copper chloride lattice greatly enhances the reactivity of copper (I), compared to that of pure CuCl. The pattern of reactivity in these carbon monoxide reactions is quite similar to that previously described for the sorptive reconstruction of $CuAlCl_4$ upon reaction with ethylene,[2] though notable contrasts in the reactivity are observed as a function of the common ion Lewis acid ($AlCl_3$ or $GaCl_3$).

Mechanistic Considerations. Though not a microporous material $CuMCl_4$ (M = Al and Ga) exhibits a remarkable sorption capacity of up to 200 cm^3 of CO or ethylene per g of sorbate. This reactivity proceeds via a reaction mechanism that we have described as sorptive reconstruction. Two one-equivalent adduct phases, described as α and *β*, respectively, are observed by powder X-ray diffraction. The sorption isotherm measurements shown in Figure 2 also give indication of reaction via two distinct pathways, consistent with the formation of these two adducts. It has not yet been possible to unequivocally determine which reaction pathway leads to which of the two **1-CO** polymorphs. However, because only the *β*-1-CO_{Ga} adduct has been observed for reaction of $CuGaCl_4$ with CO, and reactions with the gallate only exhibit the stepwise *β* path isotherms, we suggest that the stepwise sorption isotherm for alluminate material also proceeds through the formation of *β*-1-CO_{Al}. Furthermore, the pressure resolved diffraction measurements that show the formation of α-1-CO_{Al} (Figure 4) also exhibit significant and concomitant formation of **2-CO_{Al}**, whereas those showing the formation of *β*-1-CO_{Al} exhibit only trace formation of **2-CO_{Al}** (see supplemental figure S1). We therefore suggest that this reaction path, described as the α path, corresponds to the continuous sorption isotherm, shown as red squares in Figure 2.

(38) Rouquerol, F.; Rouquerol, J.; Sing, K. *Adsorption by Powders and Porous Solids*; Academic Press: London, 1999.

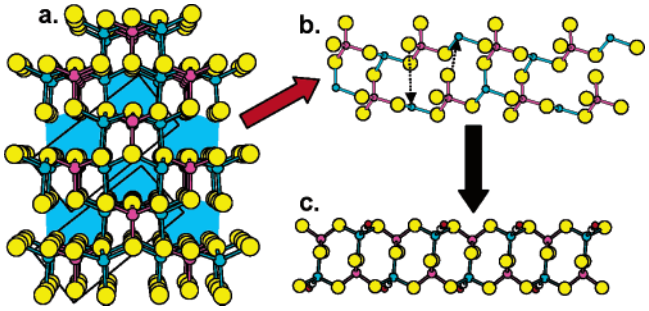

Figure 10. Pathway for the sorptive reconstruction of α-$CuAlCl_4$ to chains of (CO)$CuAlCl_4$. (a) View of α-$CuAlCl_4$ looking down the 112 vector with shaded blue regions highlighting the van der Waals channels. (b) A chain excised from α-$CuAlCl_4$ (outlined in a box in (a)) running parallel to the 112 vector. (c) A single chain of β-(CO)$CuAlCl_4$. Copper, aluminum, and chlorine atoms are colored purple, blue and yellow, respectively.

The single-crystal structure of the β-phase has been determined and found to be nearly iso-structural to that of β-(et)-$CuAlCl_4$, β-1-et. However, the slightly smaller size and end-on binding of CO, as compared to the edge binding of ethylene, results in a more efficient packing of the carbonyl ladder chains. Both ethylene and CO adduct structures can be described based on a close packing of the chlorides and ligands. However in β-1-et, 1/6 of the close-packing sites are vacant, whereas all sites are filled with either CO or Cl in β-1-CO. This results in only a 130% expansion of the unit cell volume upon formation of β-1-CO as opposed to the 150% expansion observed for the formation of β-1-et.

Upon careful examination of the crystalline structures of the parent α-$CuMCl_4$ and the product β-1-CO it is apparent that van der Waals channels through the parent crystalline phase[39] direct the reactivity toward CO. The van der Waals channels between close packed halide layers, highlighted in blue in Figure 10a, though too small for the ligand to pass through, provide the entry point for ligand attack. We have colloquially referred to this type of excision reaction as a "rat snake" mechanism, whereby the jaw of the snake is disengaged in order to accommodate swallowing an egg that is much larger than its mouth.[2] The structure shown in Figure 10b is simply a chain running along the 112 vector that has been excised from α-$CuAlCl_4$. This chain consists of two $CuAlCl_4$ units that form a four-metal ring analogous to the four-rings in the 1 equiv adduct chain, and two units that exhibit chloride bridges along the ladder rails but lack the across-chain halide bridges to form the ladder rungs. Excision of such a chain is possible with nucleophilic attack by CO at the Cu(I) center followed by an inversion of configuration that breaks select network Cu−Cl bonding. Rotation of the tetrachloraluminate building blocks, as implied by the dotted arrows in Figure 10b, allows terminal aluminum bound chlorides, released when CO is coordinated to the coppers of a neighboring chain, to form bridges to the opposite rail of the forming ladder chain. Preliminary kinetic data for ethylene sorption, assumed to be analogous to the CO sorption, suggest that the rate of this reaction increases with increasing reactive gas pressure, consistent with an associative mechanism whereby ligand coordination is the rate-limiting step; as opposed to a dissociative mechanism that would require initial Cu−Cl cleavage (defect formation) to be rate limiting, followed by ligand coordination.

(39) Martin, J. D.; Leafblad, B. R.; Sullivan, R. M.; Boyle, P. D. *Inorg. Chem.* **1998**, *37*, 1341−1346.

The structure of the α-1-CO_{Al} phase is not yet clearly defined, though as noted above, it appears to be similar to the α-1-et, phase previously reported for ethylene reactivity. Whereas the adduct chains run parallel in the β-phase, they run in orthogonal directions in the α-phase.[2] As also proposed for the ethylene reactivity, we suspect that nucleation at the tetragonal-van der Waals channels of α-$CuAlCl_4$ provide the reaction pathway that leads to the α-1-CO_{Al} product.

Exposure of either **1-CO** adduct phase to a higher pressure of CO results in the formation of the two equivalent adduct **2-CO**. As articulated in our prior description of the ethylene induced sorptive reconstruction,[2] this is accomplished by nucleophillic attack of additional CO at the copper centers and scission of the ladder chains.

The reactivity of $CuMCl_4$ toward CO when trace amounts of water are present, which result in the formation of (CO)CuCl, is in notable contrast to the afore described sorptive reconstruction mechanism. Instead of allowing the reaction to propagate down the van der Waals channels of the parent phase, the trace amount of water apparently causes a surface disproportionation of $CuMCl_4$ to nanoparticulate CuCl and some MCl_3 containing decomposition product. The near molecular dimension of CuCl provided by the decomposition of this bulk crystalline system affords reactivity with CO closer to that observed for reaction of CuCl dissolved in aqueous acid or polar organic solvents than is observed for bulk crystalline CuCl.[12,13] Apparently the formation of (CO)CuCl does not provide a sufficient driving force to overcome the lattice energy of bulk CuCl, thus precluding reactivity until CO pressures of greater than 100 atm[12] are achieved. By contrast, molecular or nanoparticulate CuCl exhibits an equilibrium binding pressure of about 0.5 atm.[13]

Lewis Acid Impact on Ligand Binding. Evaluation of the Cu−CO bonding demonstrates that in addition to the enhanced reactivity, incorporation of a strong Lewis acid into the copper chloride lattice exhibits a significant influence on the bonding of ligands. Whereas previous work clearly demonstrated particle size effects for the CO sorption into CuCl,[14] indicating a significant kinetic barrier to small molecule sorption, the addition of Lewis acids to the copper chloride lattice alters the thermodynamics and kinetics of ligand binding[16−18] such that the reactivity is relatively particle size independent. Crystal structure analysis does not exhibit extensive variation of M−C and C−O distances as a function of bonding environment. The C−O distance observed for β-1-CO_{Al} is 1.102(4) Å, compared to that observed for (CO)CuCl, 1.112(18) Å.[13b] Their respective Cu−C distances are essentially equivalent (1.856(16) Å in (CO)CuCl and 1.857(3) Å in (CO)$CuAlCl_4$). This is consistent with the suggestion that the strong Lewis acid, $AlCl_3$, decreases any ability of the Cu(I) to back-bond with the carbonyl ligand. The nonclassical nature of the Cu−CO bonding in these compounds is more clearly demonstrated by the carbonyl stretching frequency $\nu_{CO} = 2156\ cm^{-1}$, which is 13 cm^{-1} higher in energy than that of free CO ($\nu_{CO} = 2143\ cm^{-1}$). By comparison to other materials described in Table 1 above, it is clear that **1-CO_{Al}** and **1-CO_{Ga}** exhibit more nonclassical bonding than the weakly classical (CO)CuCl, $\nu_{CO} = 2120\ cm^{-1}$,[13b] but are less nonclassical than (CO)Cu[AsF_6], $\nu_{CO} = 2178\ cm^{-1}$.[17] The matrix-isolated $(CO)Cu^+$ cation, with $\nu_{CO} = 2234\ cm^{-1}$ represents the nonclassical limit for CO binding to Cu(I).[34] The bands at 2182

and 2107 cm^{-1} observed at higher CO pressures, which we assign to the dicarbonyl adduct, **2-CO$_{Al}$**, are consistent with the symmetric and asymmetric stretches of a pseudo-trigonal-planar $(CO)_2CuCl$ unit (see structure of $(et)_2CuAlCl_4$ in ref 2) rather than the linear dicarbonyl cation structure proposed for $(CO)_2Cu[AsF_6]$.[17]

As described in eq 1, a conjugate anion of a strong Lewis acid is a poor ligand to the copper center. By weakening the metal ligand bonds, i.e., from Cu−Cl to Cu−ClAlCl$_3$, the π-donor and σ-acceptor orbitals of Cu(I) are significantly lowered in energy (Figure 1), thus favoring a nonclassical mode of carbonyl binding. Though not typically reported, direct evidence of this orbital stabilization can be observed by UV/vis diffuse reflectance measurements of the Cu $d^{10} \rightarrow$ CO π^* electronic transitions. A very weak feature is observed in the UV/vis spectrum of (CO)CuCl with $\lambda_{max} = 37.8 \times 10^3$ cm^{-1}, whereas **1-CO$_{Al}$** exhibits a broad feature blue shifted to $\lambda_{max} = 38.4 \times 10^3$ cm^{-1} (equivalent spectra are observed for **1-CO$_{Ga}$**, Supplemental information Figure S4). The energy of the MLCT band does not significantly change with the sorption of more than 1 equiv of CO. Though the absorption bands are less defined than for the ethylene adducts, the strong and broad absorptions with maxima at 42.1×10^3 cm^{-1} and 48.8×10^3 cm^{-1} observed with higher CO pressure are consistent with a change in coordination about copper from pseudo tetrahedral in **1-CO** to a pseudo trigonal-planar coordination in **2-CO**.

Both IR and UV/vis spectra paint a similar picture of weakened binding of the lattice chloride ligands to copper when strong Lewis acids are incorporated. Interestingly, the ν_{CO} of both copper−aluminum and -gallium complexes is essentially equivalent to that observed for the matrix isolated linear (CO)-CuCl molecules, suggesting that the three Cu−Cl bonds in (CO)-$CuAlCl_4$ (average $d_{Cu-Cl} = 2.41$ Å) provide equivalent bonding to Cu as the single Cl ligand in the matrix isolated molecule (CO)CuCl (Cu−Cl = 2.10 Å).[24] (By way of reference the average Cu−Cl bond distance for the four contacts in CuCl is 2.35 Å[40] and 2.36 Å for the three Cu−Cl bonds in crystalline (CO)CuCl[13b]).

The variation in the copper−carbonyl bonding, described above, directly impacts the reactivity, as well as the sorption capacity of the systems. While the sorption reactions may exhibit a significant kinetic barrier (largely seen as particle size effects) due to the deconstruction of the parent crystalline lattice, the desorption isotherms are most useful for determining the strength of the copper carbonyl interactions. Previously it was shown that for the weakly classical carbonyl complex (CO)CuCl, the room-temperature equilibrium binding pressure is 440 Torr.[13a,14] While this value is reasonably sensitive to temperature, it is largely independent of the path by which it was formed (bulk, thin film, nanoparticle or solution reaction), and there is no evidence for sorption of greater than 1 equiv of CO. By contrast, the nonclassical carbonyl complexes discussed here exhibit a significantly lower equilibrium binding pressure of around 350 Torr. Both these Cu/Al and Cu/Ga materials are shown to bind a second equivalent of CO under elevated pressure, with desorption equilibrium binding pressures of between 700 and 500 Torr. Binding of CO to these adducts appears to be slightly more facile for the Cu/Al material than the Cu/Ga material, nevertheless, the latter may have a slightly lower equilibrium binding pressure. That sorption of CO into the Cu/Al system is somewhat more facile than sorption into the Cu/Ga system is attributed to fact that the melting point of the Cu/Al−CO adducts is very close to room temperature (with the eutectic below room temperature) suggesting a softer lattice. The $CuGaCl_4$ lattice is more rigid and the Cu/Ga−CO adducts decompose before they melt. The slight, but opposite trend in the equilibrium binding pressures may be a result of differential Cu−CO bonding as a result of $GaCl_3$ being a slightly weaker Lewis acid. Furthermore, based on the slope of the isotherms, it is likely that a third equivalent of CO may be bound at pressures higher than are accessible with our gas line. These results are consistent with the sorption of CO into the even more nonclassical system $CuAsF_6$ for which a one-equivalent adduct is observed to form with CO pressure of 3−10 Torr, a low melting two-equivalent adduct forms at pressures between 10 and 100 Torr, and a solid three-equivalent adduct forms at pressures between 100 and 500 Torr.[17]

It is thus clear that the bonding characteristics that are the basis of nonclassical Cu−CO bonding also can enhance the reactivity and sorption capacity of these copper(I)-based sorbates. These results further support the suggestion that it is σ-type bonding that dominates the Cu−CO binding. In this regard, it is informative to compare the reactivity of both CO and ethylene with these copper-based materials. Whereas CO is only a moderate σ-donor but an excellent π-acceptor, ethylene is a good σ-donor ligand but only a modest π-acceptor. As a result, CuCl, which allows weak π-back-bonding (it forms a weakly classical carbonyl complex), forms a stable carbonyl complex with a room-temperature dissociation pressure of 440 Torr,[13] but the dissociation pressure from (et)CuCl is about 8 atm.[10] By contrast, the nonclassical $CuAlCl_4$, for which predominatly σ-bonding is observed, forms strong ethylene adducts with dissociation pressures of < 10 Torr from **1-et$_{Al}$** and ~70 Torr from **2-et$_{Al}$**, and relatively weaker carbonyl adducts with dissociation pressures of ~360 Torr from **1-CO$_{Al}$** and ~700 Torr from **2-CO$_{Al}$**. The slightly weaker Lewis acid $GaCl_3$ (in $CuGaCl_4$) results in adducts for which the ethylene vs carbonyl binding is nearly equivalent, but with a slight preference for CO. Continuation of this trend suggests that the even more nonclassical $CuAsF_6$ should exhibit an even greater affinity for ethylene binding.

Conclusions

The reversible binding of CO by $CuAlCl_4$ and $CuGaCl_4$ has been characterized by X-ray single crystal and powder diffraction, IR and UV/vis spectroscopy, and gravimetric and volumetric adsorption studies. One and two equivalent CO-adduct phases that form by topotactic reconstruction of the $CuMCl_4$ lattice have been identified for each system. Incorporating the Lewis acids $AlCl_3$ and $GaCl_3$ into the copper chloride framework facilitates both the kinetics of CO sorption and also improves the Cu(I)−CO bond strength relative to (CO)CuCl. These systems are understood from the perspective of nonclassical metal carbonyl bonding that exhibits primarily σ-bonding interactions. The nonclassical bonding, and corresponding enhanced ligand binding, is the result of the Lewis acids weakening Cu−Cl bonding upon formation of their weakly coordinating conjugate base anions ($AlCl_4^-$ and $GaCl_4^-$). These weakly coordinating anions lower the energy of the copper's frontier orbitals, making it a more effective σ-acceptor and a

(40) Wyckof, R. W. G.; Posnjak, E. *J. Am. Chem. Soc.* **1922**, *44*, 30−36.

very weak π-back-bonder. As demonstrated by comparative carbonyl vs ethylene binding, copper(I)'s propensity to adsorb gases with different σ-donor/π-acceptor characteristics can be tuned on the basis of which Lewis acids are incorporated into its framework. Stronger Lewis acids favor adduct formation with ligands that are better σ-donors (ethylene), while better π-acid ligands (CO) will bond preferentially in a more electron-donating ligand environment.

Experimental Section

General Methods and Procedures. All manipulations were performed under an inert N_2 atmosphere in a drybox, or using Schlenk or vacuum lines. The chloride materials, CuCl[41] and α-$CuMCl_4$ (M = Al, Ga),[39] were prepared according to literature methods. Carbon monoxide gas of natural isotopic abundance, used in all experiments, was purchased from either National Welders or Aldrich.

Sorption Isotherms. Gravimetric measurements were carried out in a tared Pyrex Schlenk tube loaded with α-$CuAlCl_4$ and pressurized with 1500 of Torr N_2. After determining the total mass, the tube was evacuated and pressurized with CO at 1500 Torr and allowed to equilibrate for up to 8−12 h. Because the molecular weights of CO and N_2 are equivalent (28 g/mol) any difference in mass upon substituting CO for N_2 is due to the amount of gas sorbed by the $CuAlCl_4$. In a typical experiment, 0.5 g of $CuAlCl_4$ exhibited an increase in mass of about 0.06 g upon exposure to 1500 Torr of CO.

All barometric studies were performed on a calibrated gas/vacuum line described previously.[2] To measure adsorption isotherms, approximately 40 mg of $CuAlCl_4$ powder was placed in a Pyrex sample cup with a 2-cm^2 base. The sample was covered with a layer of dry glass wool and sealed in a stainless steel container with a volume of 26 mL. The sample container was then attached to the gas line using Swagelok connectors, and nitrogen gas was purged from the container under dynamic vacuum. The dead volume of the sample holder was measured by an N_2 isotherm prior to the experiment with reactive gas. Samples were exposed to carbon monoxide by an automated process as follows. The sample chamber was isolated from the calibrated line volume, and a predetermined gas pressure was introduced into the line. The initial dosing pressure was either 50, 100, 200, or 600 Torr, depending on the specific experiment. The valve to the sample chamber was then opened, and the gas was allowed to expand into the sample volume. The line pressure was recorded once per minute for 30 min to 1 h to ensure the system came to equilibrium. The drop in pressure due to volume expansion was determined by the Boyle's law relationship ($P_1V_1/T = P_2V_2/T$). Any further decrease in pressure is attributed to gas sorption. This process was cycled, increasing the pressure of CO in incremental steps with the step size equivalent to the initial dosing pressure, until the limit of the pressure transducer was reached at 5000 Torr. Desorption experiments were carried out manually using the same gas line. The sample chamber was isolated at a given pressure, then the pressure in the calibrated line was decreased to some lower value by exposure to vacuum. The valve to the sample chamber was then opened, and the gas was allowed to expand into the calibrated line volume. After equilibration, the pressure in excess of the Boyle's law expansion was attributed to desorption from the sample. This process was repeated until pressures below 10 Torr were achieved.

X-ray Structure Determination of (CO)$CuAlCl_4$. Single crystals of (CO)$CuAlCl_4$ were grown in situ in a capillary sealed under CO pressure. Approximately 0.050 mg of α-$CuAlCl_4$ powder was placed into a fused silica tube affixed with a Teflon stopcock on one end and a hand-drawn capillary (~2 mm in diameter) on the other. Using a gas manifold, this reaction tube was evacuated and subsequently filled with approximately 500 Torr of CO and allowed to equilibrate for 30 min. The stopcock of the tube was then closed, and the base end of the tube was suspended vertically inside a tube furnace and heated to 50 °C for several hours. At this temperature the adduct melted and flowed into the capillary portion of the tube. Once the melted adduct reached the bottom, the capillary portion of the tube was flame sealed. The capillary was again heated in a furnace at 50 °C for 3 h. The furnace was cooled 0.05 °C/min to 34 °C and remained at that temperature for 6 h. Repeating this heat/cool cycle several times produced large crystals suitable for single-crystal X-ray studies. One such capillary was mounted on a goniometer such that a large single crystal (2 mm × 2 mm × 10 mm) could be centered in the X-ray beam. Data were collected at room temperature using a Bruker-Nonius X8 Apex2 diffractometer with Mo Kα radiation. The cell lattice constants were determined using 5650 reflections with $2.50° < 2\theta < 29.29°$. Reflections were collected from the entire Ewald sphere with 2369 independent reflections measured with a mixture of ϕ and ω scans from $2.51° < \theta < 30.50°$. All of the atom positions were found using direct methods with the SHELXTL program.[42] Full-matrix least-squares calculations on 1878 unique reflections [$I > 2.0\sigma(I)$] were used in the final refinement using the SHELXTL programs. The final R factors obtained were $R = 0.0341$ and $R_w = 0.0941$.

Synchrotron Powder X-ray Diffraction. Powder X-ray diffraction experiments were performed at the National Synchrotron Light Source at Brookhaven National Laboratory on beam line X7B with a wavelength of approximately 1 Å in a Debye−Scherrer collection geometry using a *MAR345* Image Plate Detector System. The wavelength, sample-to-detector distance, titling angle of the IP, and zero shift position of the IP for the data collected were calibrated to a LaB_6 standard using the *fit2d* software package to analyze the full Debye−Scherrer rings of the MAR data.[43] Powdered samples of CuCl, $CuGaCl_4$, or $CuAlCl_4$ were mixed with dried ground fused silica and placed in a 0.7 mm fused silica capillary affixed to a gas line with Swagelok fittings and aligned on a goniometer head.[44] The CO pressure was metered with an electronically controlled gas manifold. The experimental temperature was maintained at approximately 15 °C with an Oxford cryostream. The background from a $CuAlCl_4/SiO_2$ sample was subtracted to remove amorphous diffraction intensity due to the capillary and SiO_2.

The structure of β-**1-CO_{Ga}** was characterized using the GSAS suite of programs[45] and the PXRD data ($\lambda = 0.92137$ Å, $5° < 2\theta < 35°$) from the pressure resolved experiment, a portion of which is shown in Supporting Information Figure S2. This pattern contains a mixture of α-$CuGaCl_4$ and β-**1-CO_{Ga}**. The pattern was fit to the known crystal structure of α-$CuGaCl_4$[39] and a model structure derived from the single-crystal refinement of β-**1-CO_{Al}**. A spherical harmonic (ODF) correction was required to account for the observed preferred orientation for this in situ grown sample. It was not possible to achieve successful refinement of atom positions of the CO-adduct phase. Full profile refinement of the phase ratio and lattice constant variables (with all atomic parameters fixed to those of the single-crystal values for ***β*-1-CO_{Al}**) yielded a refinement of $R = 0.0551$ and $R_w = 0.0893$.

FTIR Spectroscopy. Samples for FTIR measurements were prepared with approximately 50 mg of $CuMCl_4$ in either fused silica reaction tubes or sealed between the two KBr salt plates of an IR flow cell.

(41) Kauffman, G. B.; Fang, L. In *Inorganic Syntheses*; Holt, S. L., Jr., Ed.; McGraw-Hill: New York, 1983; Vol. XXII, p 101.

(42) Sheldrick, G. M. *SHELX*, a Program for Crystal Structure Refinement, University of Göttingen: Germany.

(43) (a) Hammersley, A. P. *FIT2D: An Introduction and Overview*; ESRT Internal Report, ESRF97HA02T. European Synchrotron Radiation Facility: Grenoble Cedex, France, 1997. (b) Hammersley, A. P. *FIT2D V9.129 Reference Manual V3.1*; ESRT Internal Report, ESRF98HA01T. European Synchrotron Radiation Facility: Grenoble Cedex, France, 1998.

(44) Norby, P. In-situ Time-Resolved Synchrotron Powder Diffraction Studies of Syntheses and Chemical Reactions. In *European Powder Diffraction*; Cernik, R. J., Delhez, R., Mittenmeijer, E. J., Eds.; Materials Science Forum, Vol. 228 until Vol. 231; Trans Tech Publications: Zürich, Switzerland, 1996; pp 147−152.

(45) (a) Toby, B. H. EXPGUI, a graphical user interface for GSAS. *J. Appl. Crystallogr.* **2001**, *34*, 210−221. (b) Larson, A. C.; Von Dreele, R. B. General Structure Analysis System (GSAS). Los Alamos National Laboratory Report, LAUR 86-748, 2004.

The KBr flow cell was not airtight and thus failed for low-pressure experiments due to sorption of atmospheric moisture. For the variable-pressure experiments the fused silica tubes were evacuated to remove the N_2 after loading with sample. Then the $CuMCl_4$ was melted in a tube furnace (at 275 °C) and subsequently rapidly cooled to room temperature while rotating the tube, such that material coated the upper part of the fused silica tube. This allowed for gravity separation of the solid and liquid phases formed in the $CuAlCl_4 + CO$ reaction. Carbon monoxide gas was introduced into the tubes using a gas/vacuum manifold. Pressures were measured using an MKS PDR-D-1 pressure transducer. All spectra were collected in situ using a Mattson Genesis II spectrophotometer.

Diffuse Reflectance UV/Vis. Diffuse reflectance measurements were carried out on a Cary 3e UV−vis spectrophotometer equipped with an integrating sphere. Spectra were measured with respect to a pressed poly(tetrafluoroethylene) powder standard. Reflectance intensities were collected as the remission function, $F(R_\infty) = (1 - R_\infty)^2/2R_\infty$ (based on Kubelka−Munk theory of diffuse reflectance)[46] versus wavenumber. For measurement of the reflectance on gas sorption/desorption, samples were prepared by grinding together approximately 0.02 g of $CuMCl_4$ or CuCl with 1.0 g of ground fused silica particles (300−800 μm) with a mortar and pestle. Powdered samples were then placed in a 1 × 10 mm cuvette that was connected to a gas/vacuum manifold.

(46) Wendlandt, W. W.; Hecht, H. G. *Reflectance Spectroscopy*; Interscience: New York, 1996; Chapter 3.

Acknowledgment. Dr. Jonathan C. Hanson is acknowledged for his support at NSLS Beamline X7B, and Dr. Paul D. Boyle for his assistance in collecting the single-crystal data. This work was supported by the NSF via Contract DMR-0305086. The research carried out at beam line X7b at BNL-NSLS was supported by Contract DE-AC02-98CH10086 with the U.S. DOE office of basic energy sciences division of chemical sciences. The NSLS is supported by the Divisions of Materials and Chemical Sciences of the DOE.

Supporting Information Available: Single-crystal X-ray crystallographic data for ***β*-1-CO_{Al}** and powder data for ***β*-1-CO_{Ga}** in CIF format; figures (S1) describing the pressure-resolved synchrotron diffraction for the formation of ***β*-1-CO_{Al}**, (S2) reaction of CO with $CuGaCl_4$, (S3) IR spectrum of the $CuAlCl_4 + CO$ reaction in the flow cell with KBr windows, and (S4) showing the pressure-resolved diffuse reflectance spectra for the reaction of CO with $CuGaCl_4$. This material is available free of charge via the Internet at http://pubs.acs.org.

JA063172Q